CaMKII-Induced Shift in Modal Gating Explains L-Type Ca^{2+} Current Facilitation: A Modeling Study

Yasmin L. Hashambhoy, Raimond L. Winslow, and Joseph L. Greenstein*
Institute for Computational Medicine, Center for Cardiovascular Bioinformatics and Modeling, and the Whitaker Biomedical Engineering Institute, the Johns Hopkins University, Baltimore, Maryland

ABSTRACT Ca^{2+}/calmodulin-dependent protein kinase II (CaMKII) plays an important role in L-type Ca^{2+} channel (LCC) facilitation: the Ca^{2+}-dependent augmentation of Ca^{2+} current (I_{CaL}) exhibited during rapid repeated depolarization. Multiple mechanisms may underlie facilitation, including an increased rate of recovery from Ca^{2+}-dependent inactivation and a shift in modal gating distribution from mode 1, the dominant mode of LCC gating, to mode 2, a mode in which openings are prolonged. We hypothesized that the primary mechanism underlying facilitation is the shift in modal gating distribution resulting from CaMKII-mediated LCC phosphorylation. We developed a stochastic model describing the dynamic interactions among CaMKII, LCCs, and phosphatases as a function of dyadic Ca^{2+} and calmodulin levels, and we incorporated it into an integrative model of the canine ventricular myocyte. The model reproduces behaviors at physiologic protein levels and allows for dynamic transition between modes, depending on the LCC phosphorylation state. Simulations showed that a CaMKII-dependent shift in LCC distribution toward mode 2 accounted for the I_{CaL} positive staircase. Moreover, simulations demonstrated that experimentally observed changes in LCC inactivation and recovery kinetics may arise from modal gating shifts, rather than from changes in intrinsic inactivation properties. The model therefore serves as a powerful tool for interpreting I_{CaL} experiments.

INTRODUCTION

With each beat of the heart, cardiac myocyte contraction and relaxation occur in response to a series of events that are initiated and coordinated by the cardiac action potential (AP). Membrane depolarization during the upstroke of the AP activates voltage-gated L-type Ca^{2+} channels (LCCs), triggering Ca^{2+} influx across the sarcolemma. This influx of Ca^{2+} triggers Ca^{2+} release from the sarcoplasmic reticulum (SR), providing the necessary signal to initiate mechanical shortening of the cell.

A number of the proteins involved in this highly coordinated process of cardiac excitation-contraction coupling (ECC) are known to be modulated by Ca^{2+}/calmodulin-dependent protein kinase II (CaMKII) (1,2). CaMKII phosphorylates a number of proteins involved in ECC, including LCCs, ryanodine receptors (RyRs), and phospholamban (PLB). The large number of potential ECC-related CaMKII targets makes it difficult to quantify how phosphorylation of each target contributes to the integrative properties of ECC and myocyte function. In addition, altered function of the CaMKII signaling pathway is thought to shape the cellular phenotype of heart failure (HF) (3–6). Acute overexpression of CaMKII in isolated rabbit ventricular myocytes results in increased Ca^{2+} spark frequency and enhanced frequency-dependent acceleration of relaxation (7). In transgenic mice, elevated CaMKII activity significantly increases action potential duration, decreases twitch shortening, and leads to dilated cardiomyopathy (8).

Studies have shown that CaMKII expression level and activity are increased in human cardiac myocytes from patients with dilated cardiomyopathy (9,10). The relationship between increased CaMKII levels and HF remains unclear. Simulations by Tanskanen et al. (11) predicted that phosphorylation-induced changes in LCC gating, similar to those caused by CaMKII-mediated LCC phosphorylation, increase the likelihood of early after-depolarizations (EADs). Anderson et al. (3) demonstrated that inhibition of CaMKII activity significantly decreased likelihood of EADs in rabbit hearts. It is possible that CaMKII alters the rate of L-type Ca^{2+} current (I_{CaL}) restitution, thereby increasing the probability of EAD initiation. It is likely that abnormal CaMKII levels also modulate I_{CaL} facilitation, the Ca^{2+}-dependent augmentation of I_{CaL} observed as a positive staircase in current amplitude in conjunction with a progressively slowed rate of current inactivation, which manifests during rapid repeated depolarizing stimuli. I_{CaL} facilitation alters the behavior of LCCs under conditions of rapid pulsing, a condition that likely occurs during tachyarrhythmia or fibrillation, and has the potential to significantly alter AP shape and duration.

Many CaMKII inhibitor experiments have demonstrated that physiological I_{CaL} facilitation is the functional result of CaMKII-mediated events (12–15). Single-channel experiments have shown that CaMKII phosphorylation of LCCs results in increased channel open probability (16). Moreover, mutation studies of CaMKII-specific LCC phosphorylation sites have demonstrated that CaMKII-mediated phosphorylation of LCCs is required for I_{CaL} facilitation (17,18). Multiple mechanisms may underlie changes in properties of I_{CaL} associated with facilitation. It has been

Submitted September 9, 2008, and accepted for publication November 21, 2008.

*Correspondence: jgreenst@jhu.edu

Editor: Michael D. Stern.

© 2009 by the Biophysical Society

0006-3495/09/03/1770/16 $2.00

doi: 10.1016/j.bpj.2008.11.055

hypothesized that an increased rate of recovery of LCCs from Ca^{2+}-dependent inactivation (CDI) underlies facilitation (15,19,20). An alternate hypothesis is that a shift in the distribution of LCCs into high-activity gating modes underlies facilitation (16). LCC gating modes are recognized discrete gating patterns. Mode 1 is the dominant form of LCC gating, and it is characterized by repeated brief openings. Mode 2 is a high-activity gating mode characterized by prolonged channel openings (21). However, it is difficult to experimentally dissect the distinct fundamental mechanisms of CaMKII-mediated LCC phosphorylation associated with I_{CaL} facilitation, because these mechanisms would be triggered by the same signal, i.e., an elevated local concentration of Ca^{2+}. Changes in either the modal distribution of LCC openings or the magnitude of CDI are closely coupled via alterations in local Ca^{2+} levels, and both of these phenomena can result in increased I_{CaL}. We hypothesize that the phosphorylation-dependent shift in LCC modal gating distribution from mode 1 to mode 2 is the primary mechanism underlying the hallmarks of I_{CaL} facilitation, namely, I_{CaL} amplitude augmentation, the apparent macroscopic increase in the rate of recovery from inactivation, and an observed slowing of the inactivation rate of whole-cell I_{CaL}. This hypothesis was tested by interpreting existing experimental data in the context of a previously validated model (22). The dynamic interactions among CaMKII, LCCs, phosphatases, and dyadic Ca^{2+} levels were modeled in the context of the canine ventricular myocyte, thus allowing us to gain a further understanding of the mechanisms underlying macroscopic phenomena such as I_{CaL} facilitation that would otherwise be difficult to obtain from experimental observations alone.

To do this, we have developed a biochemically detailed, stochastic model describing: 1), transitions between activity states in individual CaMKII monomers; 2), dynamic phosphorylation and dephosphorylation of LCCs, mediated by CaMKII and phosphatases; and 3), LCC voltage- and Ca^{2+}-dependent gating. Over the past 15 years, in vitro kinetic studies (23–25), cell-based assays (7), and transgenic mouse studies (8) have been used to investigate the structure and function of CaMKII under various conditions. A number of groups have formulated multistate CaMKII models that replicate in vitro experimental results and accurately describe the CaMKII state as a function of Ca^{2+} and calmodulin (CaM) concentration (26–28). In addition, others have developed models of CaMKII action within its physiologic environment in attempting to elucidate the role of CaMKII in neurons (29) and cardiac myocytes (30–32). The model presented here is based on this prior work, but it has been extended to reproduce integrative behaviors of CaMKII and LCCs at physiologic protein levels in cardiac myocytes. An additional novel feature of this new model is that it allows for dynamic transition of individual LCCs between gating modes, which occurs as a function of the phosphorylation state of the channel.

The model of CaMKII monomer activity is based on that created previously by Dupont et al. (26), which has been shown to faithfully reproduce dynamic in vitro experimental results on CaMKII activation. The model has been extended to include dephosphorylation reactions and two additional CaMKII activity states relating to phosphorylation at the CaM binding site. The model of CaMKII-mediated LCC phosphorylation is based on biochemical studies (17,18). It is coupled with a modified version of a Markov state model of the LCC, which accurately reproduces single-channel experimental results, and this model has been validated against whole-cell findings after incorporating it into an integrative computational model of the canine ventricular myocyte (22). Model results suggest that a CaMKII-dependent shift in LCC modal distribution is sufficient to account for increased I_{CaL} amplitude, the apparent macroscopic increase in the rate of recovery from inactivation, and the slowing of the inactivation rate observed experimentally.

METHODS

The CaMKII-LCC model

The complete model described in this work is referred to as the *CaMKII-LCC model*. It consists of three modules: the CaMKII activity model, the LCC phosphorylation model, and the LCC gating model. The CaMKII-LCC model is formulated to describe local interactions between individual CaMKII and LCC molecules.

Electron microscopy imaging and crystal structure analysis have shown that CaMKII monomers (subunits) join together to form a dodecameric holoenzyme (33–35). In addition, biochemical analysis has revealed that CaMKII tethers to the LCC and acts as an integrator of local Ca^{2+} signaling (36). The CaMKII-LCC model assumes that there is one 12-subunit holoenzyme tethered to each LCC, as proposed by Hudmon et al. (36).

The space in which CaMKII molecules and LCCs interact is a microdomain known as the dyad. Each dyad has a height of ~15 nM and a diameter of ~100 nM, as illustrated in Fig. 1. There are several thousand dyads positioned along the network of T-tubular membrane in each cardiac myocyte. The local control theory of ECC states that the opening of one or a few LCCs at a particular location in the T-tubular membrane triggers Ca^{2+} release from a small cluster of nearby RyRs in the closely apposed junctional SR membrane (37,38). LCCs and RyRs are sensitive to local Ca^{2+} levels. In the CaMKII-LCC model, each module described the dynamic transitions among states of an individual CaMKII or LCC molecule in the cardiac dyad and was simulated stochastically. All modules have been integrated into the local control canine ventricular myocyte model of Greenstein and Winslow (22).

The CaMKII activity module is based on the model of Dupont et al. (26), which describes the activity of CaMKII as a function of Ca^{2+} and CaM concentrations, and it accurately reproduced results from in vitro kinase assays (23). Their five-state deterministic model has been modified by implementing it within a stochastic framework that is constrained by the geometry of a CaMKII holoenzyme. This was accomplished by restricting CaMKII autophosphorylation events to occur only between adjacent CaMKII subunits. This change had no significant effect on simulated average in vitro CaMKII activity (see Supporting Material). The model was further modified by the addition of two more physiologic states: the capped state C, in which CaMKII is phosphorylated at both T287 and T306 (CaM binding site), and the additional inactive state U, in which CaMKII is phosphorylated only at T306, as described in Hudmon and Schulman (39). It has been shown that protein phosphatases 1 (PP1) and 2a (PP2A) are primarily responsible for dephosphorylating CaMKII sites T287 (36,40,41) and T306 (42),

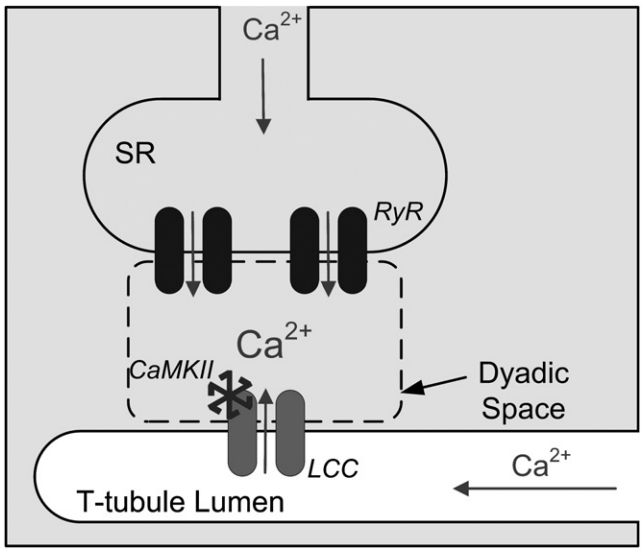

FIGURE 1 Schematic representation of the cardiac dyad. Ca^{2+} ions pass through the LCC and enter the dyad, where they bind to RyRs, triggering their opening and leading to Ca^{2+} release from the SR. A CaMKII holoenzyme is tethered to each LCC, and the activity of each CaMKII monomer is a function of dyadic Ca^{2+} levels. Ca^{2+} ions released from the SR diffuse out of the dyad into the bulk myoplasm.

respectively. These dephosphorylation reactions have been incorporated into the CaMKII activity model presented here.

Fig. 2*A* illustrates the CaMKII activity model, which reflects the different structural and functional states of the kinase, as described in Hudmon and Schulman (39). CaMKII molecules each have a catalytic, a regulatory, and an association domain. When the regulatory domain folds over the catalytic site, the kinase inhibits its own activity and is unable to phosphorylate its targets. This is called the inactive state, corresponding to state I. Autoinhibition is eliminated when Ca^{2+}-bound calmodulin (Ca/CaM) binds to the regulatory domain, thus exposing the catalytic site. This bound configuration is represented by state B. CaMKII is considered to be "active" in this state. When CaMKII is phosphorylated at T287 by an adjacent molecule in the CaMKII holoenzyme, its affinity for CaM and its kinase activity both increase. This phosphorylated configuration corresponds to state P. While it is phosphorylated at T287, a decrease in Ca^{2+} concentration will allow the bound Ca^{2+} to unbind, leaving CaMKII in a state that remains active (state T), although at a lower level of activity than that in state P. Even if CaM is released while T287 is phosphorylated (state A), CaMKII remains active. Once the kinase occupies state A, it rapidly phosphorylates itself at the binding site T306, preventing Ca^{2+}/CaM from binding again. This "capped" state, represented by state C, is far less catalytically active than any other active state (43). CaMKII remains in this dual phosphorylated active state until T287 is dephosphorylated by PP1, at which point it occupies the inactive state U. CaMKII returns back to state I upon dephosphorylation at site T306. It should be noted that the transition from inactive state I to U is a possible but rare occurrence, through a very slow autophosphorylation reaction (42).

The T287 dephosphorylation rate was derived by converting the specific activity of purified PP1 from 25,000 units of substrate phosphate/mg/min (New England Biolabs, Ipswich, MA) to a rate of 0.01561 molecules of substrate phosphate/molecule of PP1/ms. To constrain the concentration of PP1, the height of the dyadic cleft was considered (15 nM (37)). Because of the very small distance between LCCs and RyRs, it was assumed that a PP1 molecule tethered to each RyR (44,45) apposing the LCC would be able to contribute to the dephosphorylation of CaMKII. In the Greenstein and Winslow model (22), the RyR/LCC ratio is 5:1 in each dyad. Therefore, in our model, 5 PP1 molecules acted to dephosphorylate the 12 CaMKII subunits in each holoenzyme. Using this rate of dephosphorylation and CaMKII/PP1 stoichiometry in model simulations, only ~4% of CaMKII was autophosphorylated during 2-Hz pacing (see Fig. S3 in the Supporting Material). This is consistent with the negligible level of CaMKII autophosphorylation measured in response to high-frequency pacing in rat ventricular

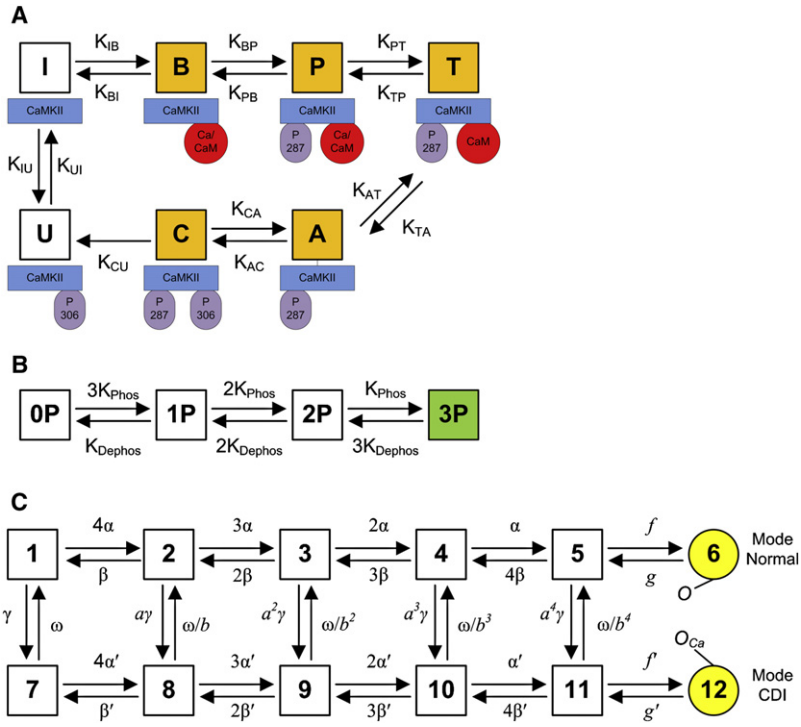

FIGURE 2 State diagrams for the CaMKII, LCC, and CaMKII-LCC modules. (*A*) State model of the activation and deactivation processes of the CaMKII activity module. Transition rates for individual CaMKII monomers are modeled as a function of Ca^{2+} levels, CaM, and phosphatase in the dyad and as a function of the activity of neighboring CaMKII subunits in the holoenzyme. States that are shaded in are active. (*B*) State model of the CaMKII-LCC phosphorylation module. Higher CaMKII activity translates into higher phosphorylation rates, thus promoting transition from the left-to-right states. Dephosphorylation is a fixed rate, modeled on PP2A activity and concentration. If a channel is phosphorylated at all three sites (*shaded*), it gates in mode 2. (*C*) State model of the voltage activation processes of the LCC channel module (22). Depolarization promotes transitions from left to right toward open states. Elevation of Ca^{2+} promotes CDI.

myocytes (40). PP2A dephosphorylates CaMKII at site T306. Additionally, it dephosphorylates the LCC. In the model, all PP2A dephosphorylation rates were assumed to be equal. A description of the data used to constrain these rates can be found in the explanation of the LCC phosphorylation model.

Ca^{2+}/CaM binding and autophosphorylation each affect the conformation of CaMKII and influence the degree to which its catalytic subunit is exposed. As a result, CaMKII phosphorylates its targets at different rates, depending on its state. Following the method of Dupont et al. (26), we defined an activity coefficient associated with each conformation, which represents the state's phosphorylation rate normalized to the maximum phosphorylation rate of CaMKII. These coefficients are listed in Table 1. The "activity" of a CaMKII molecule refers to the activity coefficient associated with its current state. The activity of a CaMKII holoenzyme, $CaMKII_{HoloAct}$, is defined as the average of the activities of its 12 subunits. This value was used to determine the phosphorylation rate of its associated LCC within each dyad.

Fig. 2 *B* illustrates the structure of the four-state Markov LCC phosphorylation model. In the figure, *i*P refers to the state in which *i* sites are phosphorylated. This model is based on mutation studies (17,18) indicating that LCCs undergo complete facilitation if and only if they are phosphorylated at each of three distinct sites (T498 on the β-subunit and S1512 and S1570 on the α-subunit). Using various peptide substrates, White et al. (46) determined the optimal recognition motif of CaMKII. It consists of hydrophobic amino acids at positions -5 and $+1$, arginine at position -3, and a nonbasic amino acid at position -2 (where positions are given with respect to the serine/threonine phosphorylation site). It was observed that if these critical sites were varied, CaMKII V_{max}/K_m decreased significantly. Because all three phosphorylation sites on the LCC are part of such optimally recognizable consensus sequences, the rate of phosphorylation of each LCC site was assumed to be equal, and was assumed to vary as a function of the average CaMKII activity of the attached holoenzyme. Currently, there are no additional data available regarding the rate of phosphorylation at these sites. The maximum phosphorylation rate of each LCC site (K_{Phos}) is assumed to be equal to the phenomenologic rate constant for phosphorylation, K_{BToP}, used by Dupont et al. (26).

It has been shown that PP2A is tethered to the LCC (47) and that this phosphatase is responsible for mediating mode 2 gating resulting from protein kinase A (PKA)-mediated phosphorylation (48). We assumed that PP2A also dephosphorylates the three CaMKII-mediated phosphorylation sites on the LCC described above. We performed a parametric analysis and set the rate of dephosphorylation (K_{Dephos}) equal to a fraction of the maximum dephosphorylation rate reported by PP2A distributors (Gentaur, Brussels, Belgium), to obtain ~15% increase in peak I_{CaL} at 2-Hz pacing, as seen in rabbit ventricular myocytes (15). Because experimental data has shown that CaMKII and PP2A are tethered to LCCs, the model assumes that a single CaMKII holoenzyme and a single PP2A molecule are always bound to the LCC, and, therefore, it does not account for binding reactions among the kinase, phosphatases, and channel. If an LCC is phosphorylated at all three sites, i.e., if the associated CaMKII-LCC phosphorylation model occupies state 3P, then it operates in mode 2. Otherwise, the LCC operates in mode 1. It was assumed that LCC phosphorylation occurs independently of voltage- and Ca^{2+}-dependent gating.

TABLE 1 CaMKII activity coefficients

Parameter	Value	Reference
C_I	0	(26)
C_B	0.75	(26)
C_P	1	(26)
C_T	0.8	(26)
C_A	0.8	(26)
C_C	0.17	(43)
C_U	0	(42)

C_x is the relative CaMKII activity in state x.

Fig. 2 *C* displays the 12-state Markov LCC gating model, originally developed by Jafri et al. (49) and later modified in the Greenstein and Winslow canine ventricular myocyte model (22). In this model, LCCs undergo voltage- and Ca^{2+}-dependent gating. States 1–6 are "mode normal," meaning that there is no inactivation by bound Ca^{2+}/CaM, and states 7–12 are "mode CDI," which denotes channel binding by Ca^{2+}/CaM. States 1–5 are normal mode closed states. Forward and reverse transition rates among these states are voltage dependent. State 6 is the mode normal open state. The parameters *f* and *g* describe the transition rates between states 5 and 6, and they are voltage independent. States 7–11 are mode CDI closed states. The transition rates among these states are voltage dependent. State 12 is open and in mode CDI. It is very rare for a channel to occupy state 12, because the constant transition rate between states 11 and 12 (f') is very small. The transition rates from normal mode closed states 1–5 to mode CDI states 7–11 increase with subspace $[Ca^{2+}]$, whereas the reverse rates are constant. Independent of these transitions, channels also undergo voltage-dependent inactivation (VDI), a process that is more than an order of magnitude slower than the rates with CDI (50,51). For a channel to be open, it must occupy state 6 or 12, and it must not be voltage inactivated.

The LCC gating model reflects two forms of channel gating, mode 1 and mode 2, which are distinguished by their mean open time. In single-channel studies on isolated murine ventricular myocyte LCCs, Dzhura et al. (16) demonstrated that phosphorylation of channels by constitutively active CaMKII results in a shift to mode 2 gating. They also showed that the mean open time for channels in mode 2 is ~20 times longer than that in mode 1. We use the original Greenstein and Winslow LCC model (22) to characterize mode 1, because it has been shown to accurately describe this form of gating. In our model, mode 2 gating is assumed to be identical to that of mode 1, except for a 20-fold reduction in the rate of channel closing from the mode normal open state, to reflect the difference in mean open time (transition rate *g*). Channels have the ability to shift dynamically between modes 1 and 2, based on their phosphorylation state, which is characterized in the LCC phosphorylation model. The phosphorylation state of the LCC is checked at all time steps while the LCC is open, and if it is in the fully phosphorylated state 3P (corresponding to all three sites phosphorylated), then the rate *g* is reduced 20-fold. This implementation allows the channel to be in either mode 1 or mode 2 (fully phosphorylated) and to be in either mode normal (not calcium inactivated) or in CDI. It will therefore be possible for some channels to be in both mode 2 and in CDI. It is important to emphasize that CDI channels have identical rates whether in mode 1 or mode 2, and, therefore, there is no real distinction between modes 1 and 2 while in CDI. The rate g' has not been altered in mode 2 channels, simply because this would have virtually no significant effect, because the CDI open state (state 12) is virtually never occupied. Single-channel studies that characterize properties of mode 1 versus mode 2 LCCs are typically performed in environments in which CDI does not occur. There is therefore no evidence to suggest how mode 1 and mode 2 channel gating properties may differ upon CDI, and, therefore, it has been assumed that there is no difference. It should be clarified that phosphorylation of the channel does not activate it; phosphorylation serves only to reduce the rate of channel closing. Therefore, if a channel is Ca^{2+}-inactivated (i.e., already closed) and phosphorylated, then the phosphorylation will not have any effect unless the channel recovers from its CDI state and occupies an open state. A list of frequently used variable names can be found in Table 2. Detailed equations and parameters describing the CaMKII-LCC model can be found in the Appendix.

Whole-cell model

The CaMKII-LCC model was integrated into the canine ventricular myocyte model of Greenstein and Winslow (22). Briefly, this model stochastically simulates the local interactions of individual LCCs with apposing RyRs, and now with CaMKII molecules, and embeds these simulations within the numerical integration of differential equations describing ionic and membrane pumps, exchangers and currents, Ca^{2+} cycling, and time-varying

TABLE 2 Frequently used variable names and abbreviations

Variable name/abbreviation	Definition
CaMKII	Calmodulin kinase II
LCC	L-type Ca^{2+} channel
RyR	Ryanodine receptor
CaM	Calmodulin
PP1	Protein phosphatase 1
PP2A	Protein phosphatase 2A
$[Ca_{cleft}]$	Ca^{2+} concentration in the dyad
C_X	CaMKII activity coefficient of state X
$CaMKII_{HoloAct}$	Average CaMKII activity over the holoenzyme
K_{XToY}	Transition rate from state X to state Y

cytosolic ion concentrations at the level of the myocyte. A 64-bit version of the Mersenne Twister algorithm was employed as the random number generator, as described in Tanskanen et al. (52). A typical simulation involves an ensemble of 1000 dyads.

RESULTS

Single-channel experiments

Our central hypothesis is that the phosphorylation-dependent shift in LCC modal gating distribution from mode 1 to mode 2 is the primary mechanism underlying I_{CaL} amplitude augmentation, the apparent macroscopic increase in the rate of recovery from inactivation, and an observed slowing of the inactivation rate of whole-cell I_{CaL}. It is therefore important to confirm that the modified LCC model presented here is consistent with single-channel experimental data. Experiments performed by Dzhura et al. (16) confirmed that CaMKII-mediated phosphorylation of LCCs results in a modal shift that increases the number of channels gating in mode 2. In these experiments, a voltage clamp was applied to LCCs in excised inside-out patches, in the presence of different bath solutions. In one set of trials, the channels were exposed to constitutively active, Ca^{2+}-independent CaMKII that was phosphorylated at the T287 site; in another set of trials, CaMKII was absent from the bath. Membrane potential was held at −70 mV for 1800 ms, followed by depolarization to a test clamp potential of 0 mV for 200 ms. Single-channel openings were recorded during each test clamp.

Statistics of measured channel open times in these experiments indicate that with constitutively active CaMKII present, 50% of the channels gated in mode 2 and 50% gated in mode 1, from which it can be assumed that one half of the LCCs were phosphorylated at all of the CaMKII-mediated sites and that the remaining LCCs were not. This is a plausible assumption, because it is possible that during some CaMKII experiments, LCCs were exposed to suboptimal levels of active kinase, resulting from incomplete thiophosphorylation of CaMKII in the generation of constitutively active kinase. (It was reported that Ca/CaM-independent CaMKII activity was 35–50% of the total activity, and this activity level persisted at >75% of initial levels during the course of the experiments.) It is also possible that protein phosphatases were not washed out completely from the excised patches. The activity of these phosphatases would serve to counteract phosphorylation by CaMKII on LCCs.

Fig. 3 illustrates results from isolated simulations, in which the CaMKII-LCC model was decoupled from the ventricular myocyte model. Fig. 3 *A* displays a histogram of LCC open durations calculated from 200 single-channel voltage clamp sweeps that were simulated in the presence of constitutively active CaMKII and in the absence of phosphatases and Ca^{2+} (because EGTA was present in the bath in experiments). Model results reproduced experimental findings with a mean open time of ~10 ms. It should be noted

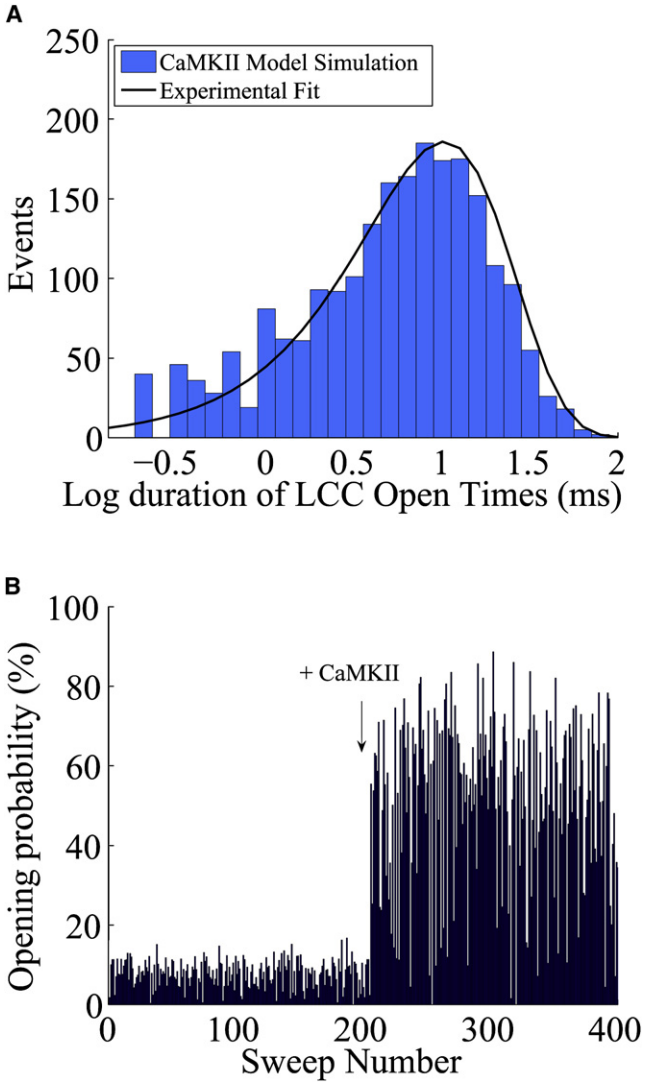

FIGURE 3 CaMKII-LCC phosphorylation model results. As in single-channel studies performed in (16), LCCs were hyperpolarized to −70 mV for 1800 ms, and then depolarized to 0 mV for 200 ms. (*A*) Single- channel open times after exposure to constitutively active CaMKII. Histogram: simulation results; curve: experimental fit, as described in (16). (*B*) Simulation results of open probabilities for individual sweeps before and after the addition of constitutively active CaMKII at sweep 201. Measurements were obtained during the depolarization period of the voltage clamp.

that the lack of Ca^{2+} precludes CDI and, consequently, more channel openings occur under these conditions than would be expected under physiological conditions.

Fig. 3 *B* shows results from a simulation in which 400 consecutive voltage clamp sweeps are applied to the LCC. The first 200 sweeps occur in the absence of CaMKII, and then constitutively active CaMKII is added to the bath before sweep No. 201. After the addition of CaMKII, a large fraction of sweeps exhibit a channel open probability that exceeds 60%, which is consistent with experimental results of Dzhura et al. (16). If the experiments of Dzhura et al. (16) are interpreted to indicate that exposure to CaMKII leads to a distribution of 50% of LCCs operating in mode 1 and 50% operating in mode 2, then the open probability of LCCs in the presence of CaMKII should equal the average of the open probabilities of mode 1 and mode 2 LCCs. The simulated open probability was found to be 7.88% when CaMKII was absent and 50.08% when it was present. The mean open probability was 28.98%, which agrees well with the experimentally obtained value of 25% (16).

I_{CaL} pulse experiments

Pacing experiments in rabbit (7,12,15), mouse (16), and rat (14,19) cardiac myocytes have indicated that CaMKII must be active for LCC facilitation to occur. After rest, when ventricular myocytes are repetitively depolarized at rates of 1–2 Hz, peak I_{CaL} increases in a staircase-like manner after the first pulse and reaches a steady state, with a peak amplitude remaining at least 10% higher than that of the first pulse until pacing ceases. However, when CaMKII-specific inhibitors such as AIP or KN-93 are applied, this positive staircase effect is eliminated.

We have been able to reproduce these results accurately in the model by employing the voltage clamp protocol used by Guo and Duff (19). The membrane is hyperpolarized to a holding potential of −80 mV for 60 s before pacing. Each pulse then consists of a −40-mV prepulse of 100-ms duration, followed by a 0-mV clamp of 200-ms duration. Fig. 4, *A* and *B* display simulation results of peak I_{CaL} as a function of pulse number at 1 Hz and 2 Hz pacing, respectively, in the presence and absence of CaMKII. Fig. 4 *A* shows that, at 1-Hz pacing in the CaMKII-LCC model, facilitation is evident by the third pulse and is maintained for the duration of the protocol. Steady-state facilitation is achieved by the fifth pulse, and it remains at ~22% for the duration of the protocol. In the absence of CaMKII, there are no mode 2 channels represented in the model, and, as expected, fractional current remains close to unity through the pulse train.

Fig. 4 *B* illustrates the effects of two opposing phenomena on LCCs, namely 1), Ca^{2+}- and voltage-dependent inactivation and 2), CaMKII phosphorylation, which leads to mode 2 gating. At 2 Hz, in the absence of CaMKII, the simulation clearly exhibits a negative staircase effect, consistent with experimental results in the presence of CaMKII inhibitors (15,19). Fig. 4 *C* displays the averaged simulation currents for the first eight pulses in the 2-Hz pacing protocol ($n = 30$). The kinetic properties of the averaged first-pulse currents are nearly identical, with peak values of 3.76 pA/pF and 3.74 pA/pF in the presence and absence of CaMKII, respectively. However, during the subsequent pulses, peak I_{CaL} decreases in simulations in the absence of CaMKII, whereas it increases when CaMKII is present. Steady state is achieved by the fifth pulse and maintained for the duration of the protocol. At the fifth pulse, I_{CaL} peaks at 4.88 pA/pF in the presence of CaMKII, compared to a peak of 3.17 pA/pF when CaMKII is absent. Steady-state facilitation at 2-Hz pacing in the presence of CaMKII is ~15%.

The negative staircase exhibited in the absence of CaMKII can be attributed to the LCC inactivation process. There is a slight increase in the amount of CDI over the duration of the protocol (66% at the end of the first pulse compared to 70% at the end of the twentieth pulse, data not shown). More significantly, rapid pacing precludes complete recovery from VDI between pulses, resulting in fewer channels available for opening (Fig. 4 *D*). One hundred percent of channels were available at the start of the first pulse, whereas incomplete recovery from VDI led to a reduction in LCC availability to 85% at the beginning of subsequent pulses.

Despite of the fact that fewer LCCs were available during pulses subsequent to pulse one, a positive staircase effect was evident in the presence of CaMKII, because there was a gradual increase in the fraction of mode 2 channels as a consequence of LCC phosphorylation. This shift to mode 2 provided an increase in open probability that overcame the decrease in availability due to incomplete recovery from VDI, and the net result was I_{CaL} facilitation. To understand how channels redistribute themselves between modes over time, Fig. 4 *E* presents the fraction of all LCCs that are open versus the fraction of all LCCs that are both open and in mode 2 during the 2-Hz pulse train. Whereas there are nearly no mode 2 channels open during the first pulse, by the fifth pulse, 4% of channels are open and gating in mode 2. This fraction constitutes more than one third of all open channels at peak I_{CaL} (only 11% of LCCs are open) and more than one half of all open channels during the late phase of I_{CaL}. As a result of the long open duration and, hence, high open probability of mode 2 LCCs, a small shift in the distribution of LCCs from mode 1 to mode 2 can greatly increase the overall open probability and, therefore, I_{CaL} amplitude, for the combined population of LCCs. Fig. 4 *F* shows the rapid rise in CaMKII activity, which is responsible for the phosphorylation of LCCs. Only a small fraction of this activity represents autophosphorylated states independent of Ca^{2+} levels (~4% of all CaMKII molecules are autophosphorylated; see Supporting Material), whereas the overwhelming majority of the CaMKII activity arises in response to the cycling of Ca^{2+} concentration levels in the dyad. Fig. 4, *G* and *H* display the fraction of LCCs gating in mode 2 during 1-Hz and 2-Hz pacing, respectively. At

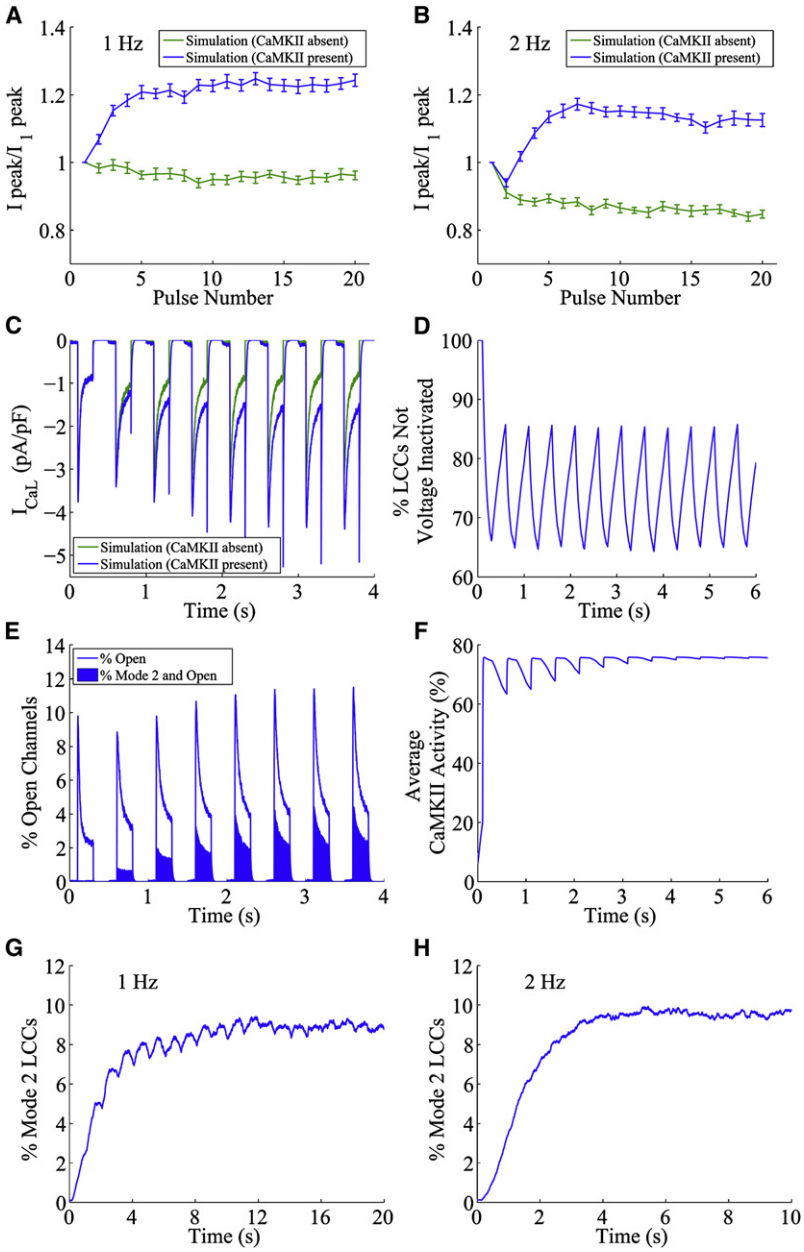

FIGURE 4 Rapid pacing simulation results. A pacing protocol was employed, as in (19), in which a prepulse of −40 mV was delivered, followed by a 200-ms depolarization to 0 mV. Holding potential was −80 mV. Twenty consecutive pulses were delivered during each trial, and 30 trials were performed for each experimental simulation ($n = 30$). Results in the presence and absence of CaMKII are presented. (*A* and *B*) Average results of peak I_{CaL} at 1Hz- and 2-Hz pacing, respectively, normalized to the peak I_{CaL} of the first pulse in the trial. Bars are mean ± SE. (*C*–*F*) Results from the 2-Hz pacing protocol, taken from model simulation results in the presence of CaMKII: (*C*) Average I_{CaL} over the first 4 s. (*D*) Average percent of LCCs not voltage inactivated over the first 6 s. (*E*) Time course of percent of total open LCCs (*solid line*) and percent of open LCCs in mode 2 only (*filled section*) during the first 4 s. (*F*) Average CaMKII activity over all CaMKII monomers during the first 6 s. (*G*) Fraction of LCCs gating in mode 2 during 1-Hz pacing. (*H*) Fraction of LCCs gating in mode 2 during 2-Hz pacing.

steady state, the fraction of total LCCs gating in mode 2 is 8.9% during 1-Hz pacing and 9.5% during 2-Hz pacing. Although a larger fraction of LCCs is gating in mode 2 during 2-Hz pacing, steady-state facilitation is lower than that at 1-Hz pacing because, at most, 85% of channels recover from VDI after the first depolarization (Fig. 4 *F*).

LCC inactivation

In rabbit adenoviral overexpression studies, Kohlhaas et al. (7) demonstrated that myocytes with a six-fold increase in CaMKII expression level display significantly slower I_{CaL} inactivation compared to that displayed by control myocytes. Maier et al. (8) made similar observations in transgenic CaMKII overexpression studies in mice. These findings seem to contradict other studies (19) that show evidence that there is no change in CDI in the presence of CaMKII and thapsigargin, which eliminates facilitation by significantly reducing SR Ca^{2+} load and, hence, subspace Ca^{2+}, thereby reducing, but not eliminating, CaMKII activation. Based on voltage clamp experiments alone, it is difficult to experimentally dissect whether CaMKII phosphorylation modulates the rate of CDI, because the increase in subspace Ca^{2+} resulting from I_{CaL} and SR Ca^{2+} release both activates CaMKII (and increases mode 2 gating) and inactivates LCCs (via CDI).

To validate the CaMKII-LCC model against experimental data and gain insight into the possible role of CaMKII in

CDI, we performed an analysis of I_{CaL} kinetics from the 1-Hz pacing protocol described in Fig. 4. It is assumed that in the experimental data (7,8), LCCs are fully recovered from inactivation at the start of each pulse. To match these conditions, the results from the 1-Hz pacing protocol simulations were used in the analysis. At 1-Hz pacing, simulations show that the entire population of LCCs is recovered from VDI at the start of each pulse. At 2-Hz pacing, VDI accumulates (Fig. 4 *D*), which would make comparison to experimental results more difficult. Fig. 5, *A* and *B* show averaged model I_{CaL} during the first pulse and the fifth to twentieth pulses, respectively. The currents are subtracted to zero steady-state current and normalized to the same peak, to visualize and compare inactivation kinetics. Fig. 5 *A* demonstrates that during the first pulse there is no noticeable difference in I_{CaL} inactivation kinetics in the presence or absence of CaMKII. However, as the pulse train progresses and facilitation develops fully (after the fourth pulse; Fig. 4 *C*), it becomes apparent that the rate of inactivation in the presence of CaMKII is slower than that in its absence (Fig. 5 *B*). To quantify this difference, the inactivation phase of each I_{CaL} curve in every simulation (i.e., from 3 ms following the peak current to steady state) is fit with a single exponential. Data from the fifth to twentieth pulses from 30 simulations were averaged both with and without CaMKII. In simulations, in the presence of CaMKII, the average time constant for inactivation is $\tau_{CaMKII} = 29.7$ ms $\pm$ 0.27 ms (mean $\pm$ SE) and, in the absence of CaMKII, $\tau_{NoCaMKII} = 24.6$ ms $\pm$ 0.13 ms. Two-way ANOVA and one-way nonparametric ANOVA Kruskal-Wallis tests both demonstrated that the time constants between the model results in the absence and presence of CaMKII are significantly different ($p < 0.0001$).

These results are similar to those reported in overexpression and transgenic mouse experiments (7,8). Whereas the difference between time constants is significant, it is relatively small (<10 ms) and may not be easily detectable in experiments that use thapsigargin to diminish facilitation (19). It should be noted that I_{CaL} simulated in the presence of CaMKII has an increased time constant of inactivation, without any modification of the intrinsic rates of voltage- or Ca^{2+}-dependent inactivation at the single-channel level. The shift in macroscopic I_{CaL} kinetics is due to CaMKII phosphorylated LCCs, which have a higher open probability than that of mode 1 channels. These results suggest that CaMKII does not necessarily alter the intrinsic CDI mechanism, contrary to the appearance of decreased inactivation dynamics in facilitated whole-cell Ca^{2+} currents.

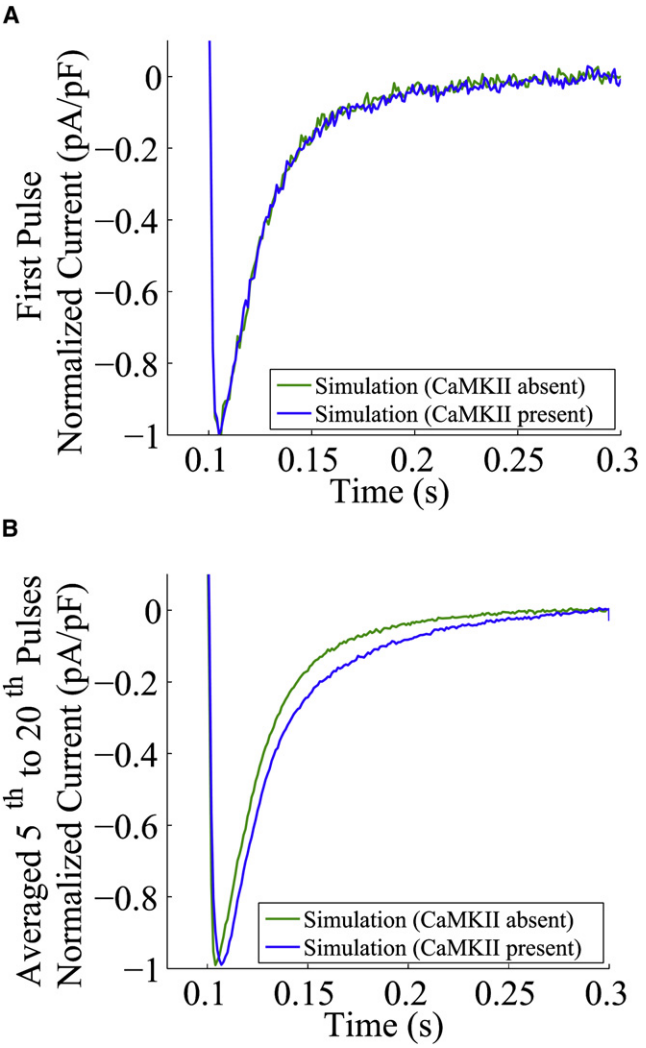

FIGURE 5 Increase in macroscopic I_{CaL} inactivation time due to shifts in modal distribution. Data are from the same 1-Hz pacing simulation as that in Fig. 4, ($n = 30$ each for each set of simulations). Averaged I_{CaL} from both sets of simulations are normalized by i) shifting the currents so that steady state is 0 pA/pF at the end of each depolarization, and then ii) multiplying the average I_{CaL} so that peak amplitudes are equal to 1 during each pulse. Results in the presence and absence of CaMKII are presented. (*A*) Normalized I_{CaL} from the first pulse in the pacing protocol. (*B*) Normalized I_{CaL} from the fifth to twentieth pulses in the pacing protocol. The kinetics of I_{CaL} between the two models are virtually identical in the first pulse; however, there is a noticeable increase in the apparent inactivation time of I_{CaL} during the fifth to twentieth pulses.

Recovery curves

Experimental studies in numerous animal models (15,19,20) have indicated that CaMKII-mediated phosphorylation modulates LCC recovery from Ca^{2+} and/or voltage-dependent inactivation. These studies employed a double-pulse protocol, in which myocytes are depolarized, then hyperpolarized for a variable length of time, and then depolarized again. Peak currents during the second pulse were measured as a function of interpulse interval and were normalized to either the peak of the current evoked by the first pulse or the peak of the current evoked on the second pulse after a sufficiently long interpulse interval.

To validate our model, we performed simulations using the same double- pulse protocol as that employed by Li et al. (20) in ferret ventricular myocytes. The SR is loaded by holding the membrane potential at −70 mV, and then

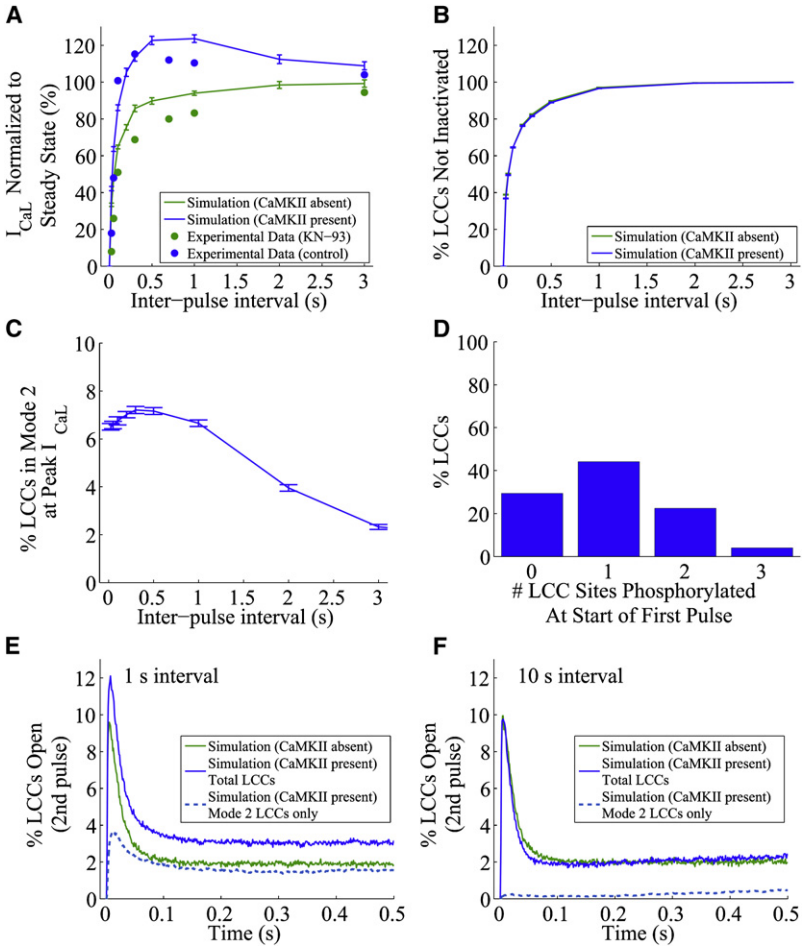

FIGURE 6 Double-pulse protocol simulation and experimental results. Membrane potential was held at −70 mV, and then depolarized to 0 mV for 200 ms at 0.5 Hz for 5 pulses to load the SR. After loading, the membrane was hyperpolarized to −90 mV for 2 s. Then for 500 ms, a depolarizing pulse to 0 mV was applied (*first pulse*), followed by hyperpolarization to −90 mV for a variable length of time, followed by another depolarizing pulse to 0 mV (*second pulse*). I_{CaL} was measured as the difference between peak current and the residual current at the end of the pulse, as in experiments (20), and normalized to peak I_{CaL} measured after a 10 s inter-pulse interval. Results in the presence and absence of CaMKII are presented. For all sets of simulations, $n = 30$ and bars represent mean ± SE. (*A*) Average normalized I_{CaL} peaks at different interpulse intervals, in CaMKII-LCC model simulations and experimental results (20). Solid lines represent simulation results. Circles represent experimental results in the presence (KN-93) and absence (control) of CaMKII inhibitor KN-93. (*B*) Model simulation results of average percentage of not-inactivated LCCs as a function of interpulse interval. (*C*) Simulation results of the fraction of mode 2 LCCs at peak I_{CaL} at each interpulse interval. (*D*) Simulation results of the fraction of LCCs phosphorylated x times at the start of the double pulse protocol ($x = 0$, 1, 2, or 3). (*E* and *F*) Average percent of open LCCs during the second pulse, at an interpulse interval equal to 1 s (*E*) or 10 s (*F*). Solid lines represent the percent of total open LCCs in simulations in the absence of CaMKII and the percent of total open LCCs (gating in both modes) in simulations in the presence of CaMKII. Dashed lines represent the percent of open, mode 2 gating LCCs in simulations in the presence of CaMKII. The fraction of open, mode 2 gating LCCs is much higher after a 1-s interval than after 10 s.

depolarizing to 0 mV for 200 ms at 0.5 Hz for five pulses. After loading, membrane potential is held at −90 mV for 2 s before applying the double-pulse protocol. A 500-ms duration pulse to 0 mV is followed by an interpulse interval at −90 mV for a variable length of time, followed by another 500-ms depolarizing pulse to 0 mV. I_{CaL} is measured as the difference between peak current and the residual current at the end of the pulse, as in experiments (20), and normalized to peak I_{CaL} measured after a 10-s interpulse interval.

Fig. 6 *A* illustrates the results obtained from simulating this protocol, superimposed upon experimental data. In simulations and experiments, when CaMKII is present, normalized peak current rises sharply, overshooting 100% at an interpulse interval of ~300 ms. The normalized peak I_{CaL} maximizes, then gradually decreases, returning almost to 100% at an interpulse interval of 3 s. In the absence of CaMKII, normalized peak I_{CaL} has a steep initial rise to 50–60% at 100 ms, and then gradually increases until it reaches 100% at an interpulse interval of ~3 s. These results suggest that CaMKII phosphorylation of LCCs results in an increased rate of LCC recovery from inactivation; however, further analysis shows otherwise (see description of Fig. 6 *B–F*). Discrepancies between experimental and simulation values may stem from the fact that recovery curves differ in their absolute values among different animal models (15,19,20).

Fig. 6 *B* presents a plot of the simulated fraction of available LCCs (i.e., channels that are not Ca^{2+}- or voltage-inactivated) as a function of interpulse interval. Clearly, whether CaMKII is absent or present, Ca^{2+} channels recover from inactivation at the same rate. This may appear to contradict the results of Fig. 6 *A*. However, the lack of effect of CaMKII in Fig. 6 *B* is expected, because no changes were made to the inactivation parameters of the original LCC gating model to simulate the action of CaMKII. The apparent inconsistencies between Fig. 6, *A* and *B* can be explained by the fact that CaMKII-phosphorylated channels stay open longer than do unphosphorylated channels. In the model, because mode 1 LCCs differ from mode 2 LCCs only by their larger closing rates, mode 2 channels have a significantly higher open probability than that of mode 1 channels (Fig. 3). Therefore, at the time of peak I_{CaL}, open probability for the population of LCCs will increase with the fraction of LCCs that are gating in mode 2. In the presence of a CaMKII inhibitor, there are no mode 2 channels and, therefore, a lower overall open probability of LCCs. The effect of this underlying mechanism on recovery curves can result in the incorrect

interpretation that there are fewer recovered channels in the presence versus the absence of CaMKII.

Fig. 6 *C* shows the averaged fraction of LCCs that are in mode 2 at the time of peak I_{CaL} during the second pulse. The curve peaks at 7.2% at an interpulse interval of 300 ms and decreases to 2.3% at an interval of 10 s. The combination of mode 2 gating (Fig. 6 *C*) and recovery from Ca^{2+}- and voltage-dependent inactivation (Fig. 6 *B*) contributes to the shape of the recovery curve in Fig. 6 *A*, in which CaMKII is present (see the Discussion section). Before the double-pulse protocol, cells undergo pacing to load the SR. This pacing activates CaMKII and leads to phosphorylation of LCCs. Fig. 6 *D* displays the distribution of LCCs partially and fully phosphorylated at the start of the double-pulse protocol. At the start of the first pulse, 4% of LCCs are gating in mode 2, and 66% of LCCs are partially phosphorylated (44% at one site and 22% at two sites). This initial state allows the fraction of LCCs in mode 2 to reach values exceeding 7% during pulse two of the double-pulse protocol (Fig. 6 *C*).

Fig. 6 *E* shows the open fraction of LCCs during pulse two, averaged over 30 simulations in the presence of CaMKII (~12% at the time of peak current) and in the absence of CaMKII (~10% at the time of peak current) when the interpulse interval is 1 s. Mode 2 channels comprise almost one third of all open channels at peak current when CaMKII is present. On the other hand, when the interpulse interval is 10 s, most CaMKII has had enough time to return to the inactive state (data not shown) and only a negligible fraction of LCCs remain phosphorylated (also not shown), leading to current amplitudes that do not differ in the presence or absence of CaMKII (Fig. 6 *F*). This small fraction of mode 2 channels has no significant effect on peak current. Our simulation results suggest that despite what appear to be convincing data from double-pulse experiments, it is not necessary to assume that CaMKII affects intrinsic rates of recovery of Ca^{2+} channels. The simpler assumption, that it promotes the transition of some LCCs from mode 1 to mode 2, leading to higher channel open probability and a greater number of open LCCs during peak current, is sufficient to explain the behaviors observed in experimental data.

DISCUSSION

In this study, we have presented a biochemically detailed, stochastic model of CaMKII activity in the cardiac ventricular myocyte. The model describes CaMKII activity as a function of Ca^{2+} levels in the dyad, dynamic phosphorylation and dephosphorylation of LCCs by CaMKII, and the functional consequences of these events on voltage- and Ca^{2+}- dependent gating of LCCs. This approach makes it possible to include information on CaMKII-phosphorylated LCC gating properties derived from single-channel experiments (16), which would otherwise be impossible when using a more phenomenologic model. The model is used to investigate the molecular basis of LCC facilitation, which is a Ca^{2+}-dependent augmentation of I_{CaL}, observed in response to rapid, repeated depolarizing stimuli. Experiments have shown that CaMKII phosphorylation of LCCs drives the channels into high-activity gating modes (16). It has also been suggested that an increased rate of recovery of LCCs from CDI underlies facilitation (15,19,20). In addition, some experimental studies have shown that CaMKII overexpression results in decreased I_{CaL} inactivation (7,8), whereas other studies have demonstrated no effect of CaMKII on CDI (19). Modeling results have shown that a broad range of experimental data on LCC facilitation can be accounted for by assuming that the major effect of CaMKII-mediated phosphorylation of LCCs is to increase the fraction gating in mode 2—a gating mode characterized by long channel open times. In this study, we have shown that a CaMKII-mediated phosphorylation of LCCs shifts the distribution LCC gating modes in favor of mode 2 channels and can account for experimentally observed increases in I_{CaL} amplitude, changes in I_{CaL} inactivation kinetics, and alterations in recovery from inactivation.

Recently, Saucerman and Bers (53) have presented a model of CaMKII activity as a function of subspace Ca^{2+}, CaM and phosphatases. Their major finding was that the different affinities of CaM for CaMKII and calcineurin determine their sensitivity to local versus global Ca^{2+} signals in the cardiac myocyte. In the modeling work described here, we have examined additional aspects of CaMKII signaling. Specifically, we have included additional physiologic CaMKII activity states and have accounted for different activity levels corresponding to each conformational state. We have also modeled the interaction between CaMKII and LCCs in the dyad, to gain an understanding of the mechanisms behind facilitation. Very importantly, we have studied CaMKII signaling using a computational model that describes graded, rather than all or none, release of Ca^{2+} from RyRs (22). The ability to describe such graded release is central to modeling and understanding Ca^{2+} signaling and regulation of LCCs in the cardiac dyad. Finally, our simulation results have been validated against dynamic pacing experimental data. This gives us confidence in our predictions of CaMKII activity under various experimental protocols.

Insights provided by model results

Pacing experiments in different animal models have shown that facilitation can range from 10–50% (12,14–16,20,54). The CaMKII-LCC model results fit well within this range. In addition, the time to reach steady-state facilitation varies among different studies. These variations may be partially due to the differences in SR Ca^{2+} uptake and SR Ca^{2+} leak among species (55,56). However, the model suggests that some of this variation can also be attributed to differences between experimental protocols. If a myocyte is hyperpolarized (allowed to rest) for a long time before initiation of

pacing, the majority of CaMKII is inactive and LCCs are completely unphosphorylated at the start of the first pulse. On the other hand, if the myocyte is repetitively depolarized to load the SR before the start of pacing, a significant fraction of CaMKII is active and some LCCs are already phosphorylated when the pacing protocol begins. In this scenario, a nonzero fraction of mode 2 channels contributes to the magnitude of I_{CaL} in response to the first pulse, thereby increasing its peak. Because facilitation is measured as a relative fractional increase of I_{CaL} with respect to the first current, an increase in first-pulse I_{CaL} results in the appearance of little-to-no facilitation. In double-pulse protocol simulations, after the membrane is repeatedly depolarized to load Ca^{2+} into the SR, and a subsequent test pulse is delivered, the fraction of mode 2 LCCs reduces to 0.343% after a 10-s interpulse interval (data not shown), compared to 6.65% after a 1-s interval, as shown in Fig. 6 *C*. This is consistent with the experimental results of Hryshko and Bers (57), who demonstrated a relationship between postrest recovery and Ca^{2+} entry by showing that 10–15 s of rest was required for fully developed I_{CaL} facilitation to occur. In the simulations shown in Figs. 4 and 5, the cell is held at the resting potential for 1 min before pacing. This is similar to the protocols used in facilitation experiments on rabbit (15) and rat myocytes (19).

Additionally, model results suggest that time of rest and Ca^{2+} entry affect experimental I_{CaL} recovery curves. If a cell is paced at high frequency before a double-pulse protocol, a subset of LCCs will be phosphorylated at the beginning of the first pulse (Fig. 6 *D*), whereas cells subjected to a long rest period before pacing exhibit little or no LCC phosphorylation. Therefore, in the former condition in which pacing occurs before the first pulse, there are likely to be more LCCs gating in mode 2 by the second pulse, thus increasing peak current and shifting the recovery curve, giving it a steeper incline. This idea would explain why, at physiologic Ca^{2+} levels, there is an overshoot in recovery curves from double-pulse experiments preceded by pacing (20), whereas no overshoot is present when the first pulse is preceded by a long period of rest (58). This idea appears to be in disagreement with results from a double-pulse experiment by Guo and Duff (19), who showed that when CaMKII was present in rat myocytes, preconditioning at a fast (1 Hz) or slow (0.1 Hz) pacing frequency had no effect on I_{CaL} recovery. However, in their experiment, the contribution of SR Ca^{2+} was eliminated by pretreatment with thapsigargin, and so it is unclear whether enough CaMKII became activated to have a significant effect on modal gating distribution and whether their conclusion can be applied to experiments in a more physiologic setting.

In the 2-Hz pacing simulation presented in Fig. 4, steady-state CaMKII autophosphorylation reached ~4% (see Fig. S3 for more details). This value is in accordance with experimental observations by Huke and Bers (40), who reported negligible levels of autophosphorylated CaMKII during high-frequency pacing. In simulations, most of the activated CaMKII is bound and unphosphorylated, which would be impossible to detect using standard CaMKII activity tests that measure T287-phosphorylation by Western blot analysis. Therefore, it is possible that actual CaMKII activity is much higher than what is typically reported in experiments. Also, if physiologic kinase activity is highly dependent on local Ca^{2+} and CaM concentrations, it is possible that CaMKII would be rendered inactive under certain patch clamp protocols, which control the intracellular cytosolic environment by rupturing the cell membrane, exposing the cytosol to the pipette solution, and significantly diluting untethered cellular proteins such as CaM. This may explain why no facilitation is reported in some pacing experiments (59), whereas, in other studies that employ perforated patch clamps (19,20), facilitation is clearly evident.

The model predicts that, during rapid pacing, the late component of I_{CaL} at the end of each depolarization is significantly greater when CaMKII is present than when it is absent (see averaged I_{CaL} curves in Fig. 4). This is a result of the high open probability of mode 2 channels. In HF, diastolic Ca^{2+} (10,60,61) and CaMKII levels (9,10) are higher than normal. It has been suggested that CaMKII overexpression acts as a compensatory mechanism for contractile dysfunction. CaMKII hyperphosphorylates PLB, which increases Ca^{2+} uptake into the SR (2,9,10). It is possible that CaMKII overexpression increases the number of CaMKII molecules that interact with LCCs in the dyad. A larger fraction of LCCs would be operating in mode 2 than the fraction under control conditions. The resulting increase of LCC Ca^{2+} flux would increase SR Ca^{2+} levels by bringing more Ca^{2+} into the cell in conjuction with enhanced SR Ca^{2+} pumping due to PLB phosphorylation. However, overexpression of CaMKII may also have proarrhythmic effects in HF, because increased mode 2 LCC gating activity may increase the likelihood of EADs (11).

Finally, a first-principles approach was taken in constructing the CaMKII activity model. The activity states C and U were added to those presented by Dupont et al. (26) to represent the full range of possible phosphorylation and binding states of the kinase. It turns out that inclusion of these additional states leads to only minor changes in the behavior of CaMKII, because these states are rarely occupied, and their contribution is small under the experimental protocols that were employed. Therefore, it may be possible to eliminate these states in future reduced model versions that simulate pacing and double-pulse protocols. However, these additional states may turn out to play an important role in other experimental protocols that were not studied in the simulations presented here.

The role of protein phosphatases

A number of studies have proposed using phosphatase inhibitors to suppress HF (62,63), and others have found that

overexpression of phosphatases impairs cardiac function (64). Model simulations indicate that protein phosphatases play a significant role in modulating LCC gating. PP1 regulates the level of Ca^{2+}-independent CaMKII levels by dephosphorylating CaMKII site T287. If PP1 levels are reduced, a higher fraction of CaMKII becomes autophosphorylated and unresponsive to surrounding Ca^{2+} levels, which indirectly limits the ability of LCCs to shift modal distribution in response to changing Ca^{2+}. Additionally, PP1 targets a PKA-specific site on the LCC that increases the rate of channel opening when it is phosphorylated (48). Therefore, a reduction in PP1 levels would also serve to increase the number of channel openings and LCC open probability.

Varying PP2A levels in the model has a significant effect on steady-state LCC mode 2 fraction and I_{CaL} facilitation during pacing (see Supporting Material). Simulations suggest that if PP2A phosphatase activity is reduced by even ~15% (possibly by detachment from LCCs or protein degradation in experiments), this would lead to an 8–9% increase in steady-state I_{CaL} facilitation. In addition, PP2A dephosphorylates a PKA phosphorylation site on LCCs that is also linked to mode 2 gating (48). A high sensitivity to PP2A could help explain some of the variation in facilitation results described earlier among different experimental groups and across species.

Model assumptions and limitations

A fundamental assumption made in the CaMKII-LCC model was that CaMKIIδ, the cardiac isoforms of the kinase, behaves in a manner similar to CaMKIIα, the isoforms commonly used in vitro experiments. This assumption was based on the fact that all isoforms share 89–93% sequence similarity in their catalytic and autoregulatory domains (65). A study of the enzymatic properties of CaMKII found that the rate of CaM binding to CaMKII was not significantly different between the α- and δ-isoforms (66). It should be noted that the same study found that half-maximal CaMKII autophosphorylation with respect to CaM was higher in α than in δ (222.6 nM vs. 123.7 nM, $p < 0.05$), but because physiologic CaM levels in the dyad are significantly higher than these half-maximal values, the autophosphorylation rate in the model was not altered to account for the differences between isoforms.

Experimental results from rabbit (15), ferret (20), and mouse (16) ventricular myocytes have demonstrated that facilitation can take place in the presence of EGTA, a Ca^{2+} chelator with slow Ca^{2+}-binding kinetics. Therefore, it is assumed in the model that the CaMKII phosphorylating LCCs solely responds to local, rapidly changing dyadic Ca^{2+} levels. However, it should be noted that an experiment by Tseng (58) showed that when EGTA concentration was reduced from 40 mM to 10 mM, or extracellular Ca^{2+} was set above physiologic levels, I_{CaL} recovery curves became steeper and in some instances displayed overshoot, such as when CaMKII activity increases and the fraction of mode 2 channels rises. Therefore, it is possible that in addition to dyadic CaMKII, cytosolic CaMKII also phosphorylates LCCs.

In the model, it is assumed that spatial constraints do not play a major role in affecting CaMKII kinetics. However, our previous studies (52) have demonstrated how packing large proteins such as RyRs and LCCs in the restricted volume of the dyad (15 nM $\times$ 100 nM) may influence properties of CICR. Whereas the small size of the cardiac dyad is at odds with the idea that large molecules could interact within the dyad, coimmunoprecipitation studies have shown that CaMKII tethers to LCCs (36), and it has been reported that many other proteins, such as PKA anchoring proteins (AKAPs), PP2A, PP1, and FK506 binding proteins, are localized within the dyad (47,67) and there may be local enrichments of mobile CaM molecules in the vicinity of each LCC (68). Structural reconstructions from electron microscopy studies of CaMKII have indicated that the diameter of the holoenzyme ranges from 14 nM to 20 nM and the height ranges from 10 nM to 20 nM, depending on the activity of the monomers (34,35). Therefore, it is possible that a holoenzyme of height 10 nM diffuses into the dyad, and that spatial constraints prevent the monomers in a holoenzyme from all activating at once. The ability of these proteins to interact and the role of geometric constraints at play in the confines of the restricted dyadic space is not well understood and deserves further study.

An important simplifying assumption made by the model is that protein phosphatase concentration and activity levels remain constant. However, it is likely that, in vivo, PP1 and PP2A activity levels change dynamically in the myocyte as a result of phosphorylation by various kinases, including CaMKII (69), inhibition by inhibitor-1 and -2 (70–72), and concentration of metalions such as Mn^{2+} and Fe^{2+} (73). However, sufficient data for modeling the dynamic behavior of these intersecting signaling pathways that activate or inhibit PP1 and PP2A is not yet available, so their levels were set to be constant.

Finally, experimental evidence demonstrates that three LCC phosphorylation sites are necessary for full facilitation. In the model, this is represented as an all-or-none phenomenon, i.e., there are no functional differences between unphosphorylated LCCs and channels that have only one or two sites phosphorylated. In addition, it was assumed that all three phosphorylation sites are dephosphorylated by PP2A at the same rate. Because it has been shown that PP2A tethers to LCCs (47) and dephosphorylates the mode 2 PKA phosphorylation site, this appears to be a reasonable assumption, given that there is no other data available. The decision to equalize the phosphorylation rates of each site is based on results from a biochemical experiment by White et al. (46), which reported an optimal substrate recognition motif for CaMKII. All three of the LCC phosphorylation sites are contained in amino acid sequences that match the optimal substrate recognition motif reported in this study.

Experimental predictions and future directions

CaMKII-LCC model simulation results predict that CaMKII-mediated phosphorylation of LCCs does not affect intrinsic CDI rates. Zühlke et al. (74) corroborated this claim by showing that facilitation and CDI are distinct forms of Ca^{2+}-dependent LCC regulation in LCC IQ motif mutation studies in *Xenopus* oocytes. However, it is unclear how much influence CaMKII would have exerted in their experimental environment. It would be interesting to test the model prediction in a more physiologic cardiac setting by applying the double-pulse protocol to cardiac myocytes with mutated LCC IQ domains that do not allow CDI. If, as hypothesized, phosphorylation by CaMKII only affects LCC gating and does not affect intrinsic CDI, then recovery curves in the presence and absence of CaMKII should be significantly different. According to our prediction, the recovery curve will be steeper for myocytes with uninhibited CaMKII, because of the higher open probability of CaMKII-phosphorylated LCCs. This effect should be even more dramatic if myocytes are paced before the double pulse to load the SR, because there will be a higher fraction of active CaMKII and phosphorylated LCCs at the start of the first pulse.

In this study, we present an original mechanistic model that examines the local interaction between individual CaMKII holoenzymes and LCCs in the context of the cardiac dyad. The model faithfully replicates single-channel, whole-cell, and in vitro results, and serves as a powerful tool for the interpretation of I_{CaL} experiments. However, in addition to LCCs, CaMKII has many targets in the cardiac myocyte, including PLB (75–77), RyRs (45,78,79), and Na^+ channels (80). Whereas it is possible that the effects of CaMKII phosphorylation on other targets may modulate intracellular ion concentrations and influence I_{CaL} facilitation, we believe that it is important to first understand the direct interaction between CaMKII and LCCs. Future studies will concentrate on the interaction between CaMKII and RyRs in an effort to interpret experimental results.

APPENDIX: STOCHASTIC MODELING

I_{CaL} was modeled in the context of the cardiac myocyte, using an integrative computational model incorporating local control of SR Ca^{2+} release, described by Greenstein and Winslow (22). In this model, local interactions of individual sarcolemmal LCCs with nearby RyRs in the JSR membrane are simulated stochastically, with these local simulations embedded within the numerical integration of the differential equations describing ionic and membrane pump/exchanger currents, SR Ca^{2+} cycling, and time-varying cytosolic ion concentrations. The stochastic component of the model was expanded to include CaMKII activity and interaction with LCCs. The state of each individual CaMKII monomer is tracked as part of the stochastic simulation. At each time step, the transition rates from the current state into different states are calculated as a function of neighboring CaMKII subunit state, subspace Ca^{2+}, PP1, PP2A, and CaM concentrations. The time that a CaMKII monomer spends in each state is exponentially distributed. Over a small time interval t_{step}, the probability of a CaMKII monomer exiting state x to enter state y ($Prob_{XtoY}$) is approximated by the time step (t_{step}) multiplied by the transition rate from state x to y (K_{XtoY}). It is ensured that t_{step} never exceeds 10% of the inverse of the largest transition rate constant. There are also additional constraints on the size of t_{step} based on dyadic Ca^{2+} levels, as described previously (22). The probability that a CaMKII monomer will leave its current state within t_{step} is equal to the sum of all exit probabilities from that state ($Prob_{SumExit}$). The probability of staying in the current state (P_{remain}) is equal to $1 - Prob_{SumExit}$. At each time step, for each CaMKII monomer, a random number ω is generated in the interval [0,1]. The subinterval in which ω dwells determines the state that the monomer will occupy next. Interval lengths correspond to the probability of entering a particular state.

For example, assume a monomer is in state N, and it can transition to state N − 1 with probability $Prob_{Nto(N-1)}$ or state N + 1 with probability $Prob_{Nto(N+1)}$, or it can remain in its current state with probability $1 - Prob_{Nto(N-1)} - Prob_{Nto(N+1)}$. If the random number ω falls in the interval $[0, 1 - Prob_{Nto(N-1)} - Prob_{Nto(N+1)}]$, then the monomer will remain in its current state. If ω lies in the interval $[1 - Prob_{Nto(N-1)} - Prob_{Nto(N+1)}, 1 - Prob_{Nto(N+1)}]$, the state will change from N to N − 1. Finally, if ω lies in the interval $[1 - Prob_{Nto(N+1)}, 1]$, the state changes from N to N + 1. This type of procedure is used to determine the transitions for all stochastic components of the ventricular myocyte model (i.e., CaMKII activity, LCC phosphorylation, LCC gating, RyR gating, and I_{to2} gating).

MODEL EQUATIONS

CaMKII activity

The equations for the CaMKII state model are as presented below. K_{XToY} defines the transition rate from state X to state Y. A list of rate parameters can be found in Table 3. Most of the rates are identical to those found in (26); however, the dephosphorylation reactions and the rates involving states C and U are new, as described earlier. In addition, a new variable $CaMKII_{HoloAct}$ is introduced. It describes the average CaMKII activity among all monomers in the holoenzyme.

$$K_{ItoU} = k_{IU} \tag{1}$$

$$K_{ItoB} = k_{IB} \times \left(Ca_4CaM_{cleft}\right) \tag{2}$$

$$K_{\mathbf{BtoI}} = k_{BI} \tag{3}$$

$$K_{BtoP} = \left(\left(Act_{MonOnLeft} + Act_{MonOnRight}\right) \times k_{BToP} \times C_B \times CaMKII^2_{HoloAct}\right)/\left(CaMKII^2_{HoloAct} + k_T^2\right), \tag{4}$$

where $Act_{MonOnLeft}$ and $Act_{MonOnRight}$ refer to the activity coefficients of the adjacent CaMKII monomers. (See Supporting Material for details on K_{BtoP}.)

$$K_{PtoB} = V_{maxPP1} \times [PP1] \tag{5}$$

$$K_{PtoT} = k_{PT} \tag{6}$$

$$K_{TtoP} = k_{TP} \times \left[Ca_{cleft}\right]^4 \tag{7}$$

$$K_{TtoA} = k_{TA} \tag{8}$$

$$K_{AtoT} = k_{AT} \times \left[CaM_{free}\right] \tag{9}$$

$$K_{AtoC} = k_{AC} \tag{10}$$

$$K_{CtoA} = \varepsilon \times V_{maxPP2A} \tag{11}$$

TABLE 3 Transition rate parameters

Parameter	Value	Reference
k_{IU}	6×10^{-7} ms^{-1}	(42)
[CaM]	0.2 mM ($\approx$ 20/dyad)	(52,68)
k_{IB}	10^{-5} nM^{-1} ms^{-1}	(26)
k_{BI}	8×10^{-4} ms^{-1}	(26)
k_{BToP}	8×10^{-4} ms^{-1}	Correspondence with authors of (26)
k_T	1.3	Correspondence with authors of (26)
k_{PT}	10^{-3} ms^{-1}	(26)
k_{TP}	10^{-3} μM^{-4} ms^{-1}	(26)
k_{TA}	8×10^{-7} ms^{-1}	(26)
k_{AT}	10^{-5} nM^{-1} ms^{-1}	(26)
k_{AC}	1.46×10^{-4} ms^{-1}	(43)
V_{maxPP1}	1.561×10^{-2}units substrate $\times$ (units PP1)$^{-1}$ ms^{-1}	New England Biolabs
[PP1]	5/12 units PP1 $\times$ (units CaMKII)$^{-1}$	(44,45); and see description of CaMKII-LCC module
$V_{maxPP2A}$	1.199×10^{-3}units substrate $\times$ (units PP2A)$^{-1}$ ms^{-1}	Gentaur Europe
ε	0.6 units PP2A $\times$ (units substrate)$^{-1}$	None (see description of CaMKII-LCC module and Supporting Material)

$$K_{CtoU} = V_{maxPP1} \times [PP1] \quad (12)$$

$$K_{UtoI} = \varepsilon \times V_{maxPP2A} \quad (13)$$

$$Ca_4CaM_{cleft} = \left([CaM] \times 10^6 \times [Ca4_{cleft}]\right)/\left([Ca4_{cleft}] + 1\right) \quad (14)$$

$$[Ca4_{cleft}] = [Ca_{cleft}]^4 \times 10^{12} \left(\text{note: } [Ca_{cleft}] \text{ is measured in nM}\right) \quad (15)$$

$$CaMKII_{HoloAct} = \frac{1}{12} \times \sum_{i=1}^{12} Act_{Monomer\ i}, \quad (16)$$

where $Act_{Monomer\ i}$ is the activity coefficient of monomer i, which is a member of the holoenzyme.

CaMKII-LCC phosphorylation

There are three putative sites on the LCC that are each phosphorylated at the same rate by CaMKII and dephosphorylated by PP2A. The transition rates are as follows:

$$K_{Phosph} = k_{BtoP} \times CaMKII_{HoloAct} \quad (17)$$

$$K_{Dephosph} = \varepsilon \times V_{maxPP2A}. \quad (18)$$

LCC gating

The details of the canine ventricular myocyte model, including the LCC gating model, can be found in (22). The only difference between mode 1 and mode 2 channels in the LCC gating model is the channel closing parameter g. When LCCs gate in mode 1, $g = 2.0$ ms^{-1}, whereas mode 2 gating LCCs have a channel closing rate, $g = 0.098$ ms^{-1}.

SUPPORTING MATERIAL

Three figures are available at http://www.biophysj.org/biophysj/supplemental/S0006-3495(09)00221-5.

This work was supported by National Heart, Lung, and Blood Institute Grant N01-HV-28180 and National Institutes of Health Grants R33HL87345 and 1P01 HL077180.

REFERENCES

1. Maier, L. S., and D. M. Bers. 2002. Calcium, calmodulin, and calcium-calmodulin kinase II: heartbeat to heartbeat and beyond. *J. Mol. Cell. Cardiol.* 34:919–939.
2. Maier, L. S., and D. M. Bers. 2007. Role of Ca^{2+}/calmodulin-dependent protein kinase (CaMK) in excitation-contraction coupling in the heart. *Cardiovasc. Res.* 73:631–640.
3. Anderson, M. E., A. P. Braun, Y. Wu, T. Lu, Y. Wu, et al. 1998. KN-93, an inhibitor of multifunctional Ca^{++}/calmodulin-dependent protein kinase, decreases early afterdepolarizations in rabbit heart. *J. Pharmacol. Exp. Ther.* 287:996–1006.
4. Wu, Y., L. B. MacMillan, R. B. McNeill, R. J. Colbran, and M. E. Anderson. 1999. CaM kinase augments cardiac L-type Ca^{2+} current: a cellular mechanism for long Q-T arrhythmias. Am. J. Physiol. Heart Circ. *Physiol.* 276:H2168–H2178.
5. Yang, Y., W. -Z. Zhu, M. -l. Joiner, R. Zhang, C. V. Oddis, et al. 2006. Calmodulin kinase II inhibition protects against myocardial cell apoptosis in vivo. Am. J. Physiol. Heart Circ. *Physiol.* 291:H3065–H3075.
6. Zhang, T., and J. H. Brown. 2004. Role of / Ca^{2+}/calmodulin-dependent protein kinase II in cardiac hypertrophy and heart failure. *Cardiovasc. Res.* 63:476–486.
7. Kohlhaas, M., T. Zhang, T. Seidler, D. Zibrova, N. Dybkova, et al. 2006. Increased sarcoplasmic reticulum calcium leak but unaltered contractility by acute camkii overexpression in isolated rabbit cardiac myocytes. *Circ. Res.* 98:235–244.
8. Maier, L. S., T. Zhang, L. Chen, J. DeSantiago, J. H. Brown, et al. 2003. Transgenic CaMKIIδC overexpression uniquely alters cardiac myocyte Ca2+ handling: reduced SR Ca2+ load and activated SR Ca2+ release. *Circ. Res.* 92:904–911.
9. Hoch, B., R. Meyer, R. Hetzer, E. -G. Krause, and P. Karczewski. 1999. Identification and expression of δ-isoforms of the multifunctional Ca^{2+}/calmodulin-dependent protein kinase in failing and nonfailing human myocardium. *Circ. Res.* 84:713–721.
10. Kirchhefer, U., W. Schmitz, H. Scholz, and J. Neumann. 1999. Activity of cAMP-dependent protein kinase and Ca^{2+}/calmodulin-dependent protein kinase in failing and nonfailing human hearts. *Cardiovasc. Res.* 42:254–261.

11. Tanskanen, A. J., J. L. Greenstein, B. O'Rourke, and R. L. Winslow. 2005. The role of stochastic and modal gating of cardiac L-type Ca^{2+} channels on early after-depolarizations. *Biophys. J.* 88:85–95.
12. Anderson, M. E., A. P. Braun, H. Schulman, and B. A. Premack. 1994. Multifunctional Ca^{2+}/calmodulin-dependent protein kinase mediates Ca^{2+}-induced enhancement of the L-type Ca^{2+} current in rabbit ventricular myocytes. *Circ. Res.* 75:854–861.
13. Wu, Y., I. Dzhura, R. J. Colbran, and M. E. Anderson. 2001. Calmodulin kinase and a calmodulin-binding 'IQ' domain facilitate L-type Ca^{2+} current in rabbit ventricular myocytes by a common mechanism. *J. Physiol.* 535:679–687.
14. Xiao, R., H. Cheng, W. J. Lederer, T. Suzuki, and E. G. Lakatta. 1994. Dual regulation of Ca^{2+}/calmodulin-dependent kinase II activity by membrane voltage and by calcium influx. *Proc. Natl. Acad. Sci. USA.* 91:9659–9663.
15. Yuan, W., and D. M. Bers. 1994. Ca-dependent facilitation of cardiac Ca current is due to Ca-calmodulin-dependent protein kinase. *Am. J. Physiol. Heart Circ. Physiol.* 267:H982–H993.
16. Dzhura, I., Y. Wu, R. J. Colbran, J. R. Balser, and M. E. Anderson. 2000. Calmodulin kinase determines calcium-dependent facilitation of L-type calcium channels. *Nat. Cell Biol.* 2:173–177.
17. Grueter, C. E., S. A. Abiria, I. Dzhura, Y. Wu, A. -J. L. Ham, et al. 2006. L-type Ca^{2+} channel facilitation mediated by phosphorylation of the β-subunit by CaMKII. Mol. *Cell.* 23:641–650.
18. Lee, T. -S., R. Karl, S. Moosmang, P. Lenhardt, N. Klugbauer, et al. 2006. Calmodulin kinase II is involved in voltage-dependent facilitation of the L-type Cav1.2 calcium channel: identification of the phosphorylation sites. *J. Biol. Chem.* 281:25560–25567.
19. Guo, J., and H. J. Duff. 2006. Calmodulin kinase II accelerates L-type Ca^{2+} current recovery from inactivation and compensates for the direct inhibitory effect of $[Ca^{2+}]i$ in rat ventricular myocytes. *J. Physiol.* 574:509–518.
20. Li, L., H. Satoh, K. S. Ginsburg, and D. M. Bers. 1997. The effect of Ca^{2+}-calmodulin-dependent protein kinase II on cardiac excitation-contraction coupling in ferret ventricular myocytes. *J. Physiol.* 501:17–31.
21. Yue, D. T., S. Herzig, and E. Marban. 1990. β-adrenergic stimulation of calcium channels occurs by potentiation of high-activity gating modes. *Proc. Natl. Acad. Sci. USA.* 87:753–757.
22. Greenstein, J. L., and R. L. Winslow. 2002. An integrative model of the cardiac ventricular myocyte incorporating local control of Ca^{2+} release. *Biophys. J.* 83:2918–2945.
23. De Koninck, P., and H. Schulman. 1998. Sensitivity of CaM kinase II to the frequency of Ca^{2+} oscillations. *Science.* 279:227–230.
24. Meyer, T., P. I. Hanson, L. Stryer, and H. Schulman. 1992. Calmodulin trapping by calcium-calmodulin-dependent protein kinase. *Science.* 256:1199–1202.
25. Miller, S. G., and M. B. Kennedy. 1986. Regulation of brain Type II Ca^{2+}/calmodulin-dependent protein kinase by autophosphorylation: a Ca^{2+}-triggered molecular switch. *Cell.* 44:861–870.
26. Dupont, G., G. Houart, and P. De Koninck. 2003. Sensitivity of CaM kinase II to the frequency of Ca^{2+} oscillations: a simple model. *Cell Calcium.* 34:485–497.
27. Hanson, P. I., T. Meyer, L. Stryer, and H. Schulman. 1994. Dual role of calmodulin in autophosphorylation of multifunctional CaM kinase may underlie decoding of calcium signals. *Neuron.* 12:943–956.
28. Kubota, Y., and J. M. Bower. 2001. Transient versus asymptotic dynamics of CaM kinase II: possible roles of phosphatase. *J. Comput. Neurosci.* 11:263–279.
29. Holmes, W. R. 2000. Models of calmodulin trapping and CaM kinase II activation in a dendritic spine. *J. Comput. Neurosci.* 8:65–86.
30. Hund, T. J., and Y. Rudy. 2004. Rate dependence and regulation of action potential and calcium transient in a canine cardiac ventricular cell model. *Circulation.* 110:3168–3174.
31. Livshitz, L. M., and Y. Rudy. 2007. Regulation of Ca^{2+} and electrical alternans in cardiac myocytes: role of CaMKII and repolarizing currents. *Am. J. Physiol. Heart Circ. Physiol.* 292:H2854–H2866.
32. Grandi, E., J. L. Puglisi, S. Wagner, L. S. Maier, S. Severi, et al. 2007. Simulation of Ca-calmodulin-dependent protein kinase II on rabbit ventricular myocyte ion currents and action potentials. *Biophys. J.* 93:3835–3847.
33. Rosenberg, O. S., S. Deindl, R. -J. Sung, A. C. Nairn, and J. Kuriyan. 2005. Structure of the autoinhibited kinase domain of CAMKII and SAXS analysis of the holoenzyme. *Cell.* 123:849–860.
34. Kolodziej, S. J., A. Hudmon, M. N. Waxham, and J. K. Stoops. 2000. Three-dimensional reconstructions of calcium/calmodulin-dependent (CaM) kinase IIα and truncated CaM kinase IIα reveal a unique organization for its structural core and functional domains. *J. Biol. Chem.* 275:14354–14359.
35. Morris, E. P., and K. Török. 2001. Oligomeric structure of α-calmodulin-dependent protein kinase II. *J. Mol. Biol.* 308:1–8.
36. Hudmon, A., H. Schulman, J. Kim, J. M. Maltez, R. W. Tsien, et al. 2005. CaMKII tethers to L-type Oligomeric structure of channels, establishing a local and dedicated integrator of Ca^{2+} signals for facilitation. *J. Cell Biol.* 171:537–547.
37. Bers, D. M. 2001. Excitation-Contraction Coupling and Cardiac Contractile Force. Kluwer Academic Publishers, Dordrecht, The Netherlands.
38. Stern, M. D. 1992. Theory of excitation-contraction coupling in cardiac muscle. *Biophys. J.* 63:497–517.
39. Hudmon, A., and H. Schulman. 2002. Structure-function of the multifunctional Ca^{2+}/calmodulin-dependent protein kinase II. *Biochem. J.* 364:593–611.
40. Huke, S., and D. M. Bers. 2007. Temporal dissociation of frequency-dependent acceleration of relaxation and protein phosphorylation by CaMKII. *J. Mol. Cell. Cardiol.* 42:590–599.
41. Schworer, C. M., R. J. Colbran, and T. R. Soderling. 1986. Reversible generation of a Ca^{2+}-independent form of Ca^{2+}(calmodulin)- dependent protein kinase II by an autophosphorylation mechanism. *J. Biol. Chem.* 261:8581–8584.
42. Colbran, R. J. 1993. Inactivation of Ca^{2+}/calmodulin-dependent protein kinase II by basal autophosphorylation. *J. Biol. Chem.* 268:7163–7170.
43. Hanson, P. I., and H. Schulman. 1992. Inhibitory autophosphorylation of multifunctional Ca^{2+}/calmodulin- dependent protein kinase analyzed by site-directed mutagenesis. *J. Biol. Chem.* 267:17216–17224.
44. Marx, S. O., S. Reiken, Y. Hisamatsu, M. Gaburjakova, J. Gaburjakova, et al. 2001. Phosphorylation-dependent regulation of ryanodine receptors: a novel role for leucine/isoleucine zippers. *J. Cell Biol.* 153:699–708.
45. Wehrens, X. H. T., S. E. Lehnart, S. R. Reiken, and A. R. Marks. 2004. Ca^{2+}/calmodulin-dependent protein kinase II phosphorylation regulates the cardiac ryanodine receptor. *Circ. Res.* 94:e61–e70.
46. White, R. R., Y. -G. Kwon, M. Taing, D. S. Lawrence, and A. M. Edelman. 1998. Definition of optimal substrate recognition motifs of Ca^{2+}-calmodulin-dependent protein kinases IV and II reveals shared and distinctive features. *J. Biol. Chem.* 273:3166–3172.
47. Davare, M. A., M. C. Horne, and J. W. Hell. 2000. Protein phosphatase 2A is associated with class C L-type calcium channels (Cav1.2) and antagonizes channel phosphorylation by cAMP-dependent protein kinase. *J. Biol. Chem.* 275:39710–39717.
48. Wiechen, K., D. T. Yue, and S. Herzig. 1995. Two distinct functional effects of protein phosphatase inhibitors on guinea-pig cardiac L-type Ca^{2+} channels. *J. Physiol.* 484:583–592.
49. Jafri, M. S., J. J. Rice, and R. L. Winslow. 1998. Cardiac Ca^{2+} dynamics: the roles of ryanodine receptor adaptation and sarcoplasmic reticulum load. *Biophys. J.* 74:1149–1168.
50. Linz, K. W., and R. Meyer. 1998. Control of L-type calcium current during the action potential of guinea-pig ventricular myocytes. *J. Physiol.* 513:425–442.
51. Peterson, B. Z., C. D. DeMaria, and D. T. Yue. 1999. Calmodulin is the Ca^{2+} sensor for Ca^{2+}-dependent inactivation of L-type calcium channels. *Neuron.* 22:549–558.
52. Tanskanen, A. J., J. L. Greenstein, A. Chen, S. X. Sun, and R. L. Winslow. 2007. Protein geometry and placement in the cardiac

dyad influence macroscopic properties of calcium-induced calcium release. *Biophys. J.* 92:3379–3396.

53. Saucerman, J. J., and D. M. Bers. 2008. Calmodulin mediates differential sensitivity of CAMKII and calcineurin to local Ca^{2+} in cardiac myocytes. *Biophys. J.* 95:4597–4612.
54. Peineau, N., D. Garnier, and J. A. Argibay. 1992. Rate dependence of action potential duration and calcium current in isolated guinea-pig cardiocytes. *Exp. Physiol.* 77:615–625.
55. Bassani, J. W., R. A. Bassani, and D. M. Bers. 1994. Relaxation in rabbit and rat cardiac cells: species-dependent differences in cellular mechanisms. *J. Physiol.* 476:279–293.
56. Bers, D. M. 2000. Calcium fluxes involved in control of cardiac myocyte contraction. *Circ. Res.* 87:275–281.
57. Hryshko, L. V., and D. M. Bers. 1990. Ca current facilitation during postrest recovery depends on Ca entry. Am. J. Physiol. Heart Circ. *Physiol.* 259:H951–H961.
58. Tseng, G. N. 1988. Calcium current restitution in mammalian ventricular myocytes is modulated by intracellular calcium. *Circ. Res.* 63:468–482.
59. Winslow, R. L., J. Rice, S. Jafri, E. Marban, and B. O'Rourke. 1999. Mechanisms of altered excitation-contraction coupling in canine tachycardia-induced heart failure, II: model studies. *Circ. Res.* 84:571–586.
60. Beuckelmann, D. J., M. Nabauer, and E. Erdmann. 1992. Intracellular calcium handling in isolated ventricular myocytes from patients with terminal heart failure. *Circulation.* 85:1046–1055.
61. Gwathmey, J. K., L. Copelas, R. MacKinnon, F. J. Schoen, M. D. Feldman, et al. 1987. Abnormal intracellular calcium handling in myocardium from patients with end-stage heart failure. *Circ. Res.* 61:70–76.
62. Pathak, A., F. del Monte, W. Zhao, J. -E. Schultz, J. N. Lorenz, et al. 2005. Enhancement of cardiac function and suppression of heart failure progression by inhibition of protein phosphatase 1. *Circ. Res.* 96:756–766.
63. Yamada, M., Y. Ikeda, M. Yano, K. Yoshimura, S. Nishino, et al. 2006. Inhibition of protein phosphatase 1 by inhibitor-2 gene delivery ameliorates heart failure progression in genetic cardiomyopathy. *FASEB J.* 20:1197–1199.
64. Gergs, U., P. Boknik, I. Buchwalow, L. Fabritz, M. Matus, et al. 2004. Overexpression of the catalytic subunit of protein phosphatase 2A impairs cardiac function. *J. Biol. Chem.* 279:40827–40834.
65. Tobimatsu, T., and H. Fujisawa. 1989. Tissue-specific expression of four types of rat calmodulin-dependent protein kinase II mRNAs. *J. Biol. Chem.* 264:17907–17912.
66. Gaertner, T. R., S. J. Kolodziej, D. Wang, R. Kobayashi, J. M. Koomen, et al. 2004. Comparative analyses of the three-dimensional structures and enzymatic properties of α-, β-, γ-, and δ-isoforms of Ca2+-calmodulin-dependent protein kinase II. *J. Biol. Chem.* 279: 12484–12494.
67. Marx, S. O., S. Reiken, Y. Hisamatsu, T. Jayaraman, D. Burkhoff, et al. 2000. PKA phosphorylation dissociates FKBP12.6 from the calcium release channel (ryanodine receptor): defective regulation in failing hearts. *Cell.* 101:365–376.
68. Mori, M. X., M. G. Erickson, and D. T. Yue. 2004. Functional stoichiometry and local enrichment of calmodulin interacting with Ca^{2+} channels. *Science.* 304:432–435.
69. Fukunaga, K., D. Muller, M. Ohmitsu, E. Bakó, A. A. DePaoli-Roach, et al. 2000. Decreased protein phosphatase 2A activity in hippocampal long-term potentiation. *J. Neurochem.* 74:807–817.
70. Freesia, L., and W. H. G. Huang. 1976. Separation and characterization of two phosphorylase phosphatase inhibitors from rabbit skeletal muscle. *Eur. J. Biochem.* 70:419–426.
71. Endo, S., X. Zhou, J. Connor, B. Wang, and S. Shenolikar. 1996. Multiple structural elements define the specificity of recombinant human inhibitor-1 as a protein phosphatase-1 inhibitor. *Biochemistry.* 35:5220–5228.
72. Blitzer, R. D., J. H. Connor, G. P. Brown, T. Wong, S. Shenolikar, et al. 1998. Gating of CaMKII by cAMP-regulated protein phosphatase activity during LTP. *Science.* 280:1940–1943.
73. Egloff, M. -P., P. T. W. Cohen, P. Reinemer, and D. Barford. 1995. Crystal structure of the catalytic subunit of human protein phosphatase 1 and its complex with tungstate. *J. Mol. Biol.* 254:942–959.
74. Zuhlke, R. D., G. S. Pitt, R. W. Tsien, and H. Reuter. 2000. Ca^{2+}-sensitive inactivation and facilitation of L-type Ca^{2+} channels both depend on specific amino acid residues in a consensus calmodulin-binding motif in the α 1C subunit. *J. Biol. Chem.* 275:21121–21129.
75. Bilezikjian, L. M., E. G. Kranias, J. D. Potter, and A. Schwartz. 1981. Studies on phosphorylation of canine cardiac sarcoplasmic reticulum by calmodulin-dependent protein kinase. *Circ. Res.* 49:1356–1362.
76. Kirchberger, M. A., and T. Antonetz. 1982. Calmodulin-mediated regulation of calcium transport and (Ca^{2+} + Mg^{2+})- activated ATPase activity in isolated cardiac sarcoplasmic reticulum. *J. Biol. Chem.* 257:5685–5691.
77. Le Peuch, C. J., J. Haiech, and J. G. Demaille. 1979. Concerted regulation of cardiac sarcoplasmic reticulum calcium transport by cyclic adenosine monophosphate dependent and calcium-calmodulin-dependent phosphorylations. *Biochemistry.* 18:5150–5157.
78. Lokuta, A. J., T. B. Rogers, W. J. Lederer, and H. H. Valdivia. 1995. Modulation of cardiac ryanodine receptors of swine and rabbit by a phosphorylation-dephosphorylation mechanism. *J. Physiol.* 487:609–622.
79. Witcher, D. R., R. J. Kovacs, H. Schulman, D. C. Cefali, and L. R. Jones. 1991. Unique phosphorylation site on the cardiac ryanodine receptor regulates calcium channel activity. *J. Biol. Chem.* 266:11144–11152.
80. Wagner, S., N. Dybkova, E. C. L. Rasenack, C. Jacobshagen, L. Fabritz, et al. 2006. Ca^{2+}/calmodulin-dependent protein kinase II regulates cardiac Na^{+} channels. *J. Clin. Invest.* 116:3127–3138.